CHEMISTRY
AN ASIAN JOURNAL
www.chemasianj.org

## Accepted Article

**Title:** Substituent Effects in BODIPY in Live Cell Imaging

**Authors:** Sandip V. Mulay, Tesla Yudhistira, Minsuk Choi, Youngsam Kim, Jinjoo Kim, Yoon Jeong Jang, Sangyong Jon, and David G. Churchill



**To be cited as:** *Chem. Asian J.* 10.1002/asia.201601400

**Link to VoR:** http://dx.doi.org/10.1002/asia.201601400

A Journal of
ACES Asian Chemical Editorial Society

A sister journal of Angewandte Chemie and Chemistry – A European Journal

WILEY-VCH

10.1002/asia.201601400


WILEY-VCH

# Substituent Effects in BODIPY in Live Cell Imaging

Sandip V. Mulay,[a,b] Tesla Yudhistira,[b] Minsuk Choi,[c] Youngsam Kim,[a,b] Jinjoo Kim,[c] Yoon Jeong Jang,[b] Sangyong Jon[c] and David G. Churchill*[a,b]

**Abstract:** Small molecule organoselenium-based fluorescent probes possess great capacity in understanding biological processes through detection of various analytes such as reactive oxygen/nitrogen species (ROS/RNS), biothiols (cysteine, homocysteine, and glutathione), and lipid droplets etc. Herein, we present how substituents in the BODIPY system play a significant part in the detection of biological important analytes for in vitro conditions and live cell imaging studies. The fluorescence of the probe was quenched by 2-chloro and 6-phenyl selenium groups; the probe shows high selectivity with NaOCl among other ROS/RNS, and gives a *turn-on* response. The maximum fluorescence intensity is attained within ~1-2 min with a low detection limit (19.6 nM), and shows a ~110 *fold* fluorescence enhancement compared with that signal generated for other ROS/RNS. Surprisingly, in live cell experiments, the probe specifically located and accumulated in lipid droplets and showed a fluorescence *turn-on* response. We believe, this *turn-on* response is because of aggregation-induced emission (AIE) which fascinated us due to only introducing one lipophilic mesitylene group at the *meso* position of the BODIPY.

## Introduction

Hypochlorous acid (HOCl) is a highly reactive oxygen species (ROS) produced in the body as a means of a defense mechanism against various pathogens and plays important roles in signaling and homeostatic control.[1] HOCl is well known as a main immune system-related chemical compound that has an effect on a broad range of microorganisms during antibacterial processes.[2] Endogenous HOCl is generated through reaction between chloride ions ($Cl^-$) and hydrogen peroxide ($H_2O_2$) which is catalyzed by myeloperoxidase (MPO) in leukocytes including macrophages, monocytes, and neutrophils.[3] It is also known as an oxidizing agent that can react easily with biological molecules such as thiol (cysteine, homocysteine, and glutathione), as well as thioethers (such as methionine). Hypochlorous acid is the most well-known bacterial oxidant to be produced by the neutrophil;[4] however, the antimicrobial agent property of HOCl also has a risk of damaging tissue through the same processes that is used to eliminate invading microorganisms.[5] Thus, an excess amount of HOCl in the body can cause several human diseases such as inflammatory diseases (e.g., arthritis),[6] hepatic ischemia reperfusion,[7] atherosclerosis,[8] neuron degeneration and death (e.g., Alzheimer's disease),[9] lung injury,[10] and cardiovascular diseases.[11]

Lipid droplets (LDs) are well known as ubiquitous organelles that preserve and provide neutral lipids such as triglycerides, steryl esters, and retinyl esters in all eukaryotic cells and several prokaryotic cells.[12] LDs can be found in the cytoplasm of normal cells, such as adipocytes and cells which are involved in protein trafficking and protein maturation.[13] The size of LDs varies from 20 to 100 mm (in white adipocytes).[14] These lipids can be used for signaling as well as membrane components, or as a source of energy.[15] LDs have a central core of hydrophobic (neutral) lipids that are surrounded by a single layer of amphipathic lipids and proteins to separate the aqueous and organic phases.[16] It is well known that lipid droplets play important roles in the immune system and have a role to exchange proteins with the nucleus in the cell and help modulate protein stability; since, LDs have sites of synthesis of eicosanoids important for defense against pathogens and cancer. These properties allow lipid droplets to act as entities that might modulate proteins to interact with binding partners, promote assembly of protein complexes, preserve the damaged proteins before protein decay, or in delivering the proteins.[17] Lipid droplets can also separate healthy and toxic lipids in the cells. For example, LDs can turn overabundant fatty acids into triglycerides and incorporated into lipid droplets which are relatively inert, stable, and harmless to protect membrane integrity. This protective function is possibly the reason for the high concentration of lipid droplets in many diseases characterized by the abnormal level of lipid supply and metabolism in such cells.[13] To date, LDs are the hallmarks of several common human diseases such as, foam cells in atherosclerotic plaques, hepatic parenchymal cells in fatty liver, and obesity which occurs because the imbalance of the lipid consumption and lipid storage.[18] In the cells, LD accumulation is heterogeneous even between identical cells;[19] it is well known that intracellular and extracellular stresses trigger LD formation in the cells.[20] Thus, accumulation of LDs can occur during progression of pathologies which are, or which are not related to lipids, such as cardiomyopathies, neuropathies, or during viral hepatitis caused by the human immunodeficiency virus.[21] Aberrations in neutral lipid storage in LDs have been associated with the development and progression of several common metabolic diseases, including obesity, type II diabetes, atherosclerosis, and Chanarin-Dorfman Syndrome.[22] Despite these ties with diseases, LDs have received little attention, and

[a] Dr. S. V. Mulay, Y. Kim, Prof. Dr. D. G. Churchill
Center for Catalytic Hydrocarbon Functionalizations, Institute for Basic Science (IBS), Daejeon, 305−701, Republic of Korea.
[b] Dr. S. V. Mulay, T. Yudhistira, Y. Kim, Y. J. Jang, Prof. Dr. D. G. Churchill
Molecular Logic Gate Laboratory, Department of Chemistry, Korea Advanced Institute of Science and Technology (KAIST), Daejeon, 305–701, Republic of Korea.
E-mail: dchurchill@kaist.ac.kr.
[c] Dr. M. Choi, J. Kim, Prof. Dr. S. Jon
Department of Biological Sciences, Korea Advanced Institute of Science and Technology (KAIST), Daejeon, 305–701, Republic of Korea.

Supporting information for this article is given via a link at the end of the document.((Please delete this text if not appropriate))

as a result, our knowledge of these organelles is limited. Therefore, there is a significant interest in designing highly sensitive and selective probes for detection of analytes such as ROS/RNS, biothiols, lipid droplets etc.

Detection methods such as potentiometric,[23] coulometric titrations,[24] and amperometric methods[25] have several drawbacks such as high detection limits (LOD) and require relatively long procedures and expensive devices to obtain results. On the other hand, a fluorescence technique offers high sensitivity, rapid in response, non-invasiveness, and can be used for in-vivo biological cellular imaging.[26] To-date, there are numbers of fluorescent small molecular probes that have been synthesized for the detection of HOCl; however, only a few among these can be used for real-time detection in biological investigations. The reason for these limitations is because of issues such as low selectivity, sensitivity, poor photostability and/or chemostability and high probe molecular weight. As a well-known and widely-used fluorophore, the BODIPY class has many compelling characteristics including an intense absorption profile, a sharp fluorescence emission spectrum, negligible triplet-state formation, high fluorescence quantum yield, good photochemical stability, good tolerance to pH, stability to a variety of physiological conditions, and chemical robustness.[27]

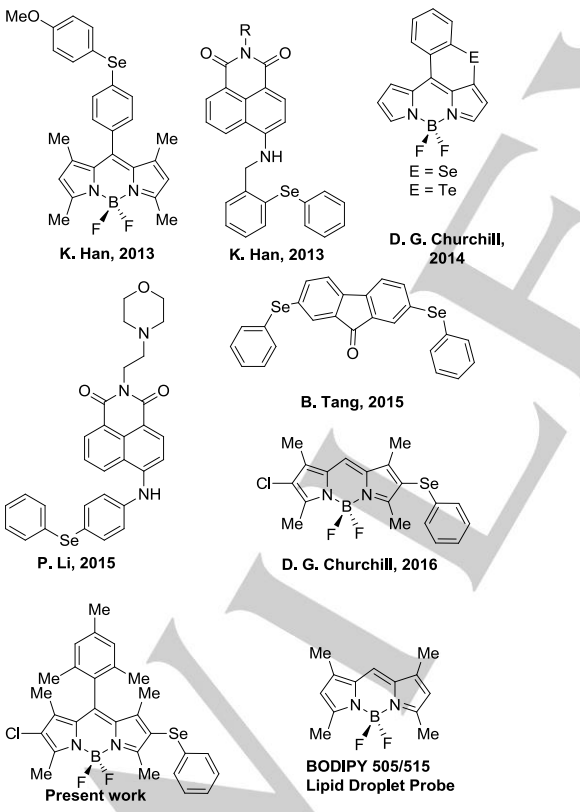


**Figure 1.** Selenium-based small molecular probes for detection of HOCl and commercially available lipid droplets probe.

Several functional groups such as thiol compounds (thioether, internal thioester, and thiosemicarbazide),[28] oxidation-hydrolysis of dibenzoylhydrazine into dibenzoyl diimide,[29] *p*-methoxyphenol,[30] oxime,[31] dibenzylhydrazine hydroquinone, and chalcogenide (S, Se, and Te)[32] systems as well as some other groups[33] display high oxidation properties that can be used as HOCl reactive moieties. These HOCl-reactive moieties are embedded onto the fluorophore to modulate the fluorescence intensity in accordance with the HOCl concentration present. Among the rest of the functional groups, oxidation of an organoselenide and telluride to the corresponding oxide by HOCl offers a rapid response and the ability for reversibility upon addition of biothiol; thus, it is a very reliable system as a probe since it is based on the redox cycle of selenium and tellurium which can provide dynamic, real time detection of HOCl with "turn-on" signalling.

In continuation, to synthesize novel chalcogenide (Se, and Te)-containing fluorescent probes[32h, 34] for the detection of biologically important species (e.g. biothiols, ROS/RNS, and metal ions), our research group has reported a novel heterocyclic annulated BODIPY (boron-dipyrromethene) systems of (selenium and tellurium atoms help form a six-membered heterocycle between the 1-position of BODIPY and *ortho* position of the *meso* phenyl ring) for the detection of HOCl via oxidation of E to E=O (E= Se/Te).[34a] Very recently, we reported simple BODIPY with 2-chloro, and 6-phenyl selenium groups that can be used for real-time detection of HOCl in biological systems. Incorporating a Cl at the 2-position in the BODIPY framework helps further decrease background fluorescence, lowers the detection limit, compared to the probe in which H is at this position.[32h]

In this work, we present a *meso* mesitylene-BODIPY embedded with a chloro and phenyl selenide at the 2- and 6-positions, respectively, and the substituent effect on the BODIPY for the detection of biological important analyte (HOCl) which involves in vitro conditions and live cells imaging studies (Figure 1, representative organoselenium probes for HOCl). The mesitylene group increases the photostability due to its electron donating character; these correlate with the steric hindrance established by the two *ortho*-substituted methyl groups inhibit free rotation of the BODIPY core and *meso* aryl group. Thus, restricting torsional motion decreases the rate of internal conversion to non-radiative decay. The effect is then increasing its fluorescence quantum yield.[35] Based on our previous work, we introduced chlorine at the 2-position and phenyl selenide at the 6-position to decrease the background fluorescence of the **Mes-BOD-SePh**. In the absence of HOCl, the fluorescence of **Mes-BOD-SePh** is quenched due to photo-induced electron transfer (PET) process by substitution of the heavy atom in the 2- and 6- positions and shows negligible fluorescence and no decrease in quantum yield of the oxidized product. The present paper reports the highly sensitive, selective and photo-stable organoselenium-based probe (**Mes-BOD-SePh)** for hypochlorous acid. As expected, the **Mes-BOD-SePh** exhibited large HOCl-induced fluorescence enhancement with a rapid response, high selectivity and comparatively wide pH detection range under in vitro conditions. But, surprisingly injecting **Mes-**

**BOD-SePh** in live cells, it shows a *turn-on* response. Though careful studies, we have demonstrated that because of the lipophilic mesitylene group probe helps target into lipid droplets and behaves with a *turn-on* response due to aggrigation induced emission (AIE).

## Results and Discussion

The synthesis of **Mes-BOD-SePh** is outlined in Scheme 1. The commercially available 2,4,6-trimethylbenzaldehyde (**1**) was treated with 2,4-dimethylpyrrole in the presence of a catalytic amount of trifluroacetic acid (TFA) under argon; subsequent oxidation with DDQ and then triethylamine, and finally $BF_3OEt_2$ afforded the BODIPY product (**2**). The monochlorination of **2** with *N*-chlorosuccinimide in hexafluoro-2-propanol (HFIP) as the solvent to give **3**, with subsequent reaction with phenylselenyl chloride delivered the probe **Mes-BOD-SePh**. The characterization of the structure of **Mes-BOD-SePh** was aided by spectroscopic techniques (multinuclear NMR spectral data, mass spectrometry, IR; Figures S1–S19, Supporting Information).

Results from the study of UV-visible and fluorescent spectroscopy with the probe are shown in Figure S20 (Supporting Information) The analysis of UV-visible spectra (3.0 μM solution of **Mes-BOD-SePh** in EtOH/ 10 mM PBS pH 7.4, 1:2 v/v) shows an absorbance at 523 nm. However, upon addition of NaOCl (4.0 equiv) to the **Mes-BOD-SePh** solution, the absorbance peak undergoes a blue shift (towards lower wavelength) at 512 nm. The non-oxidized phenylselenium group at the 6-position of the BODIPY helps quench the fluorescence of the system by a photo-induced electron transfer (PET) process. Moreover, the **Mes-BOD-SePh** shows further lower background fluorescence intensity because of the added effect from chlorine at the 2-position.

**Mes-BOD-SePh** selectivity was checked by screening with ROS/RNS solutions (e.g., NaOCl, $H_2O_2$, $^tBuO_2H$, ·OH, $^tBuO$·, $O_2^{\cdot-}$, NO, and $ONOO^-$) under physiological pH (EtOH / 10 mM PBS, pH 7.4, 1:2 v/v) in 3.0 μM of **Mes-BOD-SePh** (Figure 2). Excellent selectivity of the **Mes-BOD-SePh** is shown in Figure 2. **Mes-BOD-SePh** was found to be only selective to NaOCl (4.0 equiv) and there was no change in fluorescence intensity with other ROS/RNS even at higher concentrations (up to 100 equiv). Addition of NaOCl to the probe gives a rise in the emission to form a maximum at 526 nm with enhancement of fluorescence intensity found to be ~110-fold. The fluorescence quantum yield ($\Phi_F$) of the **Mes-BOD-SePh** was 0.0016, which is related to the

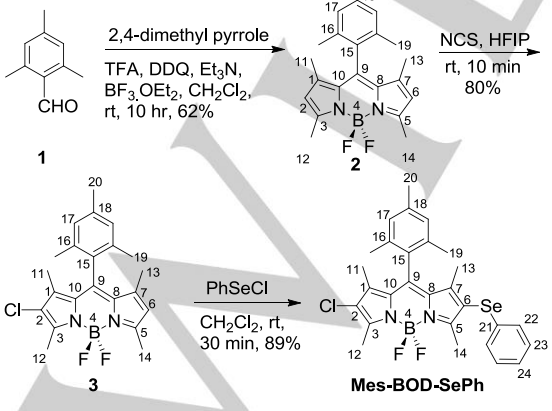


**Scheme 1.** Synthesis of **Mes-BOD-SePh**.

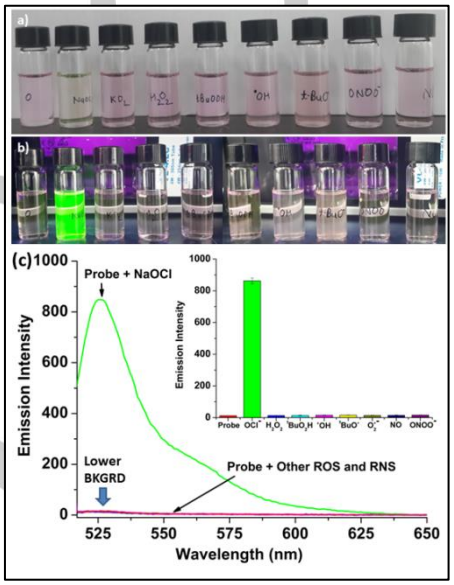


**Figure 2.** Selectivity of **Mes-BOD-SePh** with ROS/RNS; a) under visible light; b) under UV-light, $\lambda_{ex}$: 365 nm; c) Fluorescence emission spectra of **Mes-BOD-SePh** (3.0 μM) with ROS/RNS (NaOCl, $H_2O_2$, $^tBuO_2H$, ·OH, $^tBuO$·, $O_2^{\cdot-}$, NO, and $ONOO^-$) in the solution (EtOH / 10 mM PBS, pH 7.4, 1:2 v/v) incubated for 5.0 min. $\lambda_{ex}$: 512 nm, $\lambda_{em}$: 526 nm, slit width 1.5 nm/1.5 nm, Inset: solution of **Mes-BOD-SePh** (3.0 μM) with ROS/RNS (NaOCl, $H_2O_2$, $^tBuO_2H$, ·OH, $^tBuO$·, $O_2^{\cdot-}$, NO, and $ONOO^-$) in the solution (EtOH / 10 mM PBS, pH 7.4, 1:2 v/v).

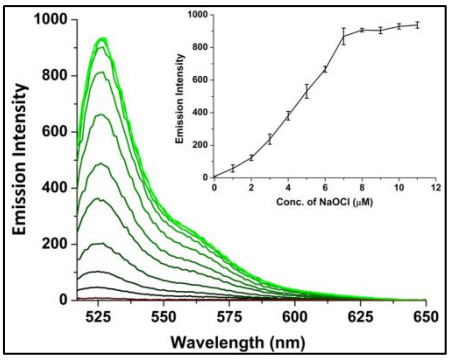


**Figure 3.** Emission spectral changes of **Mes-BOD-SePh** (3.0 μM) with various concentrations of NaOCl (0 – 3.3 equiv) in solution (EtOH / 10 mM PBS, pH 7.4, 1:2 v/v) incubated for 5.0 min, $\lambda_{ex}$: 512 nm, $\lambda_{em}$: 526 nm, slit width 1.5 nm/1.5 nm; Inset: Plot of emission intensity of **Mes-BOD-SePh** (3.0 μM) with different concentration of NaOCl in the solution (EtOH / 10 mM PBS, pH 7.4, 1:2 v/v).

incorporation of chlorine and phenylselenyl in the 2- and 6-positions, respectively. However upon addition of NaOCl, the fluorescence quantum yield ($\Phi_F$) was significantly increased to 0.45 (average of three independent experiments). The interference study of NaOCl with other ROS/RNS was performed. This result suggests that the other ROS/RNS interference studies showed no other species gave observable emission properties for **Mes-BOD-SePh** (Figure S21, Supporting Information).

Next, titration experiments of **Mes-BOD-SePh** solutions to the various concentration of NaOCl (0 to 3.3 μM) were performed; the result shows emission intensity of **Mes-BOD-SePh** solution gradually increased upon the addition of NaOCl from 0 to 3.3 equiv and was found to be linearly proportional to concentration of NaOCl. (Figure. 3, inset shows triplicate experiments). The **Mes-BOD-SePh** emission intensity reached to saturation after the addition of 2.3 equiv of NaOCl. Further studies shows that the detection limit of the probe (3σ/k, where σ stands for standard deviation of 10 blank samples measurements and k is the slope of linear equation) were determined to be 19.6 nM (Figure S22, Supporting Information).

Further time-dependent studies of the **Mes-BOD-SePh** were carried out with the addition of 4.0 equiv of NaOCl. This probe shows very fast responses upon the addition of NaOCl and gives a full strong fluorescence within 1-2 minutes (Figure 4). The result of the time-dependent experiments indicate that oxidation of selenide to selenoxide by the addition of NaOCl is very fast and can be applied to real-time sensing of NaOCl at the cellular level. To demonstrate the effect of the pH, the **Mes-BOD-SePh** was tested under wide range of pH (4 to 12). The pH studies show that, pH of the solution does not give effects to the probe under acidic conditions (Figure S23, Supporting Information). Addition of 4.0 equiv of NaOCl to the **Mes-BOD-SePh** solution at various pH values shows that the **Mes-BOD-SePh** gives a strong emission intensity under acidic conditions; however, under very base conditions the (pH 11 and 12) the emission intensity decreased significantly. These results indicated that the **Mes-BOD-SePh** can be used to measure NaOCl in the cancer cells, which is well known to have higher concentration of HOCl compared to normal cells.

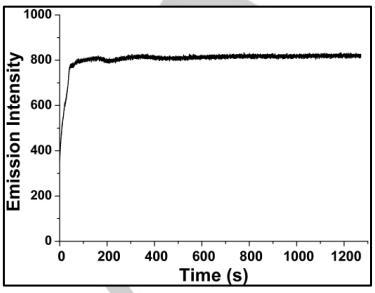


**Figure 4.** Time-dependent emission spectral changes of **Mes-BOD-SePh** (3 μM) with 4.0 equiv of NaOCl in solution (EtoH/ 10mM PBS pH 7.4, 1:2 v/v); $\lambda_{ex}$: 512 nm, $\lambda_{em}$: 526 nm.

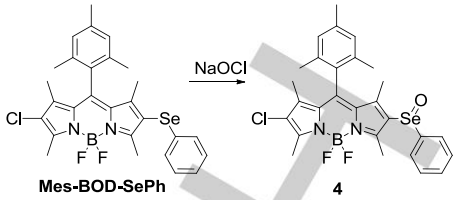


**Scheme 2.** Reaction mechanism for the detection of NaOCl.

It was previously reported that hypochlorite oxidizes selenium to selenoxide rapidly in aqueous media, as well as in organic solvents. To confirm the sensing mechanism of NaOCl based on this hypothesis (oxidation of selenium to selenoxide), the $^{1}H$ and $^{77}Se$ NMR spectra of **Mes-BOD-SePh** before and after treatment with NaOCl were recorded as the direct product of reaction. The $^{1}H$ NMR spectrum shows a downfield shifting of the phenyl protons from δ = 7.11–7.20 ppm to 7.45–7.50 and 7.61–7.63 ppm (Figure S24, Supporting Information). Also, the $^{77}Se$ NMR spectrum, after addition of NaOCl, shows a sharp peak at δ = 205.4 ppm which disappeared, leading to a new concomitant downfield peak at δ = 822.0 ppm (Figure S25, Supporting Information). Also, HRMS data of isolated compound **4** was recorded. The molecular formula of the oxidized compound **4** was $C_{28}H_{28}BClF_2N_2OSeNa$ (m/z: calcd: 595.1014; found: 595.1022, Figure S26, Supporting Information). These NMR and HRMS results strongly support that clear selenoxide formation has taken place (Scheme 2).

In order to understand the redox cycling capacity of their selenium in the **Mes-BOD-SePh**, the solutions of **4** (oxidised with hypochlorite) were treated with biothiols (gluthathione, *N*-acetyl-L-cysteine, homocysteine, and L-cysteine**)**, which are well known for it ability to revert the selenium oxide species Se=O to its original reduced state. Figure S27 (Supporting Information) shows the reaction of the oxidised product (**4**) with biothiols after 1 and 3 h. The results obtained showed a significant decrease in fluorescence intensity with gluthathione, *L*-cysteine, and *N*-acetyl-*L*-cysteine after 3.0 hours of incubation. This result indicates that the **Mes-BOD-SePh** has a reversibility**,** which is an important attribute for monitoring the dynamic variations of hypochlorite in living systems.

To confirm the photomechanism, density functional theory (DFT) geometry optimizations and time-dependent density functional theory (TDDFT) calculations were performed. The phenylselenium moiety is nearly perpendicular to the BODIPY core in its optimized structure of **Mes-BOD-SePh** (Figure S28, Supporting Information). However, electron transfer between the selenium center and the BODIPY core could be efficient because of the directly attached selenium on the 6-position of the mesitylene-BODIPY. As seen in Figure S29, (Supporting Information) electronic distributions of HOMO and HOMO-1 of the **Mes-BOD-SePh** showed very similar features occupying both BODIPY and phenylselenium. The electronic distributions on phenylselenium assigned with quenched fluorescence

because the largest oscillator strength of the **Mes-BOD-SePh** was found to have a value of $f$ = 0.5479 from HOMO-1 to LUMO (CI = 62.1 %) and HOMO to LUMO (CI = 30.2%) (Table S1, Supporting Information). On the other hand, the electron transfer from phenylselenium to the BODIPY core of the oxidized probe (compound **4**) could be less because the electronic distributions seen in the HOMO and LUMO levels showed on BODIPY core only. The largest oscillator strength is found to be $f$ = 0.3459 (HOMO – LUMO with CI = 47.7%, HOMO-1 – LUMO with CI = 47.5%). From these results, the fluorescence 'turn-on' event would be explained by a blocking of the PET that would ordinarily exist between phenylselenium and the BODIPY core by oxidation of selenium.

Finally, to show biological applications of **Mes-BOD-SePh** in live cell imaging, we choose human adipose stem cells to use in demonstrations of chemosensing. Under physiological conditions (pH 7.4, PBS buffer) the selective reaction of probe with NaOCl gave a strong green fluorescence. When human adipose stem cells were treated with the probe, followed by incubation of 30 min, the cells were expected to be non-fluorescent. But surprisingly, we observed strong green fluorescence. Compared to our previous result (*meso* unsubstituted BODIPY which are non-fluorescent in cells),[32h] the rigid and lipophilic mesitylene moiety at the *meso* position of BODIPY appears to direct the strong green fluorescence. The observed green fluorescence could exist because of aggregation of the probe; by carefully observing fluorescence images, the probe appears to selectively target lipid droplets. The selective targeting of LDs is thought to be because of the lipophilic mesitylene moiety at the *meso* position of BODIPY. A "*turn-on*" fluorescence response is then achieved by an aggregation induced emission process. To confirm that our probe selectively goes into lipid droplets, and shows fluorescence by AIE, we treated cells with a commercially-available lipid droplet staining dye (BODIPY 505/515).[36] Figure 5 shows, the fluorescence shown by the probe consistent with the lipid droplet staining BODIPY dye. These results suggest that the mesitylene group helps carry the probe into the lipid droplet; then AIE shows green fluorescence. Interestingly, here, a single heavy atom-containing group (-SePh) is not able to suitably quench the system. Therefore, we have appreciated how sterics, by way of the optical signal, can override chalcogen quenching as seen in cellular imaging. We are assuming that the Se is not oxidized, and that the -SePh group is not cleaved.

The fluorescence intensity for most of the traditional probes is highly dependent and sensitive to the working concentration of the probes. Low concentration will cause photobleaching after several scans; whereas too high concentrations will weaken the fluorescence intensity by aggregation caused quenching (ACQ). To check the impact of the concentration, human adipose stem cells were incubated with different concentration of **Mes-BOD-SePh** (1, 2.5, 5, 10, 25 μM) (Figure 6). After incubation for 30 min, the dot-shaped LDs with bright green emissions were observed, and the strong fluorescence made the probe clearly distinguishable from the background data. These results demonstrate that the **Mes-BOD-SePh** can be used at a much

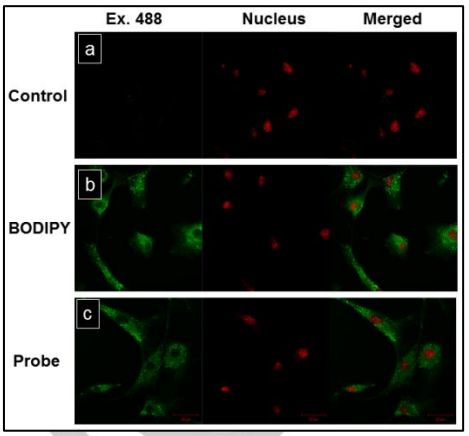


**Figure 5.** Confocal fluorescence images of human adipose stem cells incubated with (a) Non-treated control; (b) BODIPY 505/515 (10 μM) for 4 h; (c) Mes-BOD-SePh (1 μg/mL) for 4 h; Scale bar: 50 μm.

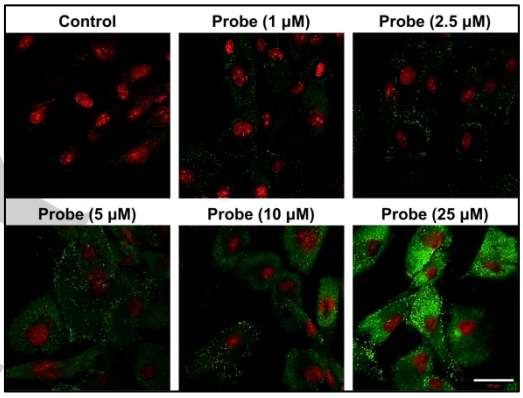


**Figure 6.** Confocal fluorescence images of human adipose stem cells incubated with various **Mes-BOD-SePh** concentration (0, 1, 2.5, 5, 10, 25 μM) for 30 min. Green: **Mes-BOD-SePh** probe, Red: nucleus stained with DRAQ5; Scale bar: 50 μm.

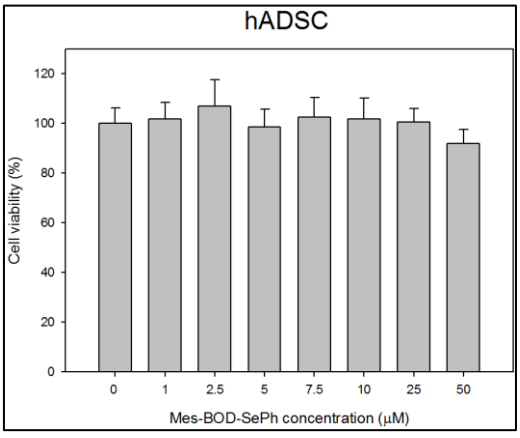


**Figure 7.** Concentration-dependent WST-1 cell viability assays. Human adipose stem cells were pre-incubated with various concentrations of **Mes-BOD-SePh** for 2 h (bar graph data is an average of three experiments).

wider concentration range to detect LDs than other reported probes.[37]

Furthermore, cell viability testing was performed to confirm the biocompatibility of **Mes-BOD-SePh**. The human adipose stem cells were pre-incubated with various concentrations of **Mes-BOD-SePh** (1, 2.5, 5, 7.5, 10, 25, 50 μM). WST-1 cell proliferation assays were carried out after cells were pre-incubated in **Mes-BOD-SePh** for 2 h. As demonstrated through Figure 7, there is no substantial decrease in cell viability when using **Mes-BOD-SePh**. These results reveal no significant cytotoxicity of **Mes-BOD-SePh** at concentrations of up to 50 μM for 2 h and help give a more full understanding for their potential biological applications.

The AIE feature of **Mes-BOD-SePh** was investigated in tetrahydrofuran (THF)/water mixture, and the measured fluorescence emission spectrum is exhibited in Figure 8. The **Mes-BOD-SePh** shows weak emission in THF and the emission intensity is almost the same up to THF/water mixture (3:7) and greatly enhanced as THF/water mixture (1:9). Since **Mes-BOD-SePh** is insoluble in water, it should have aggregated into aqueous medium. The enhanced emission intensity is thus induced by aggregate formation, demonstrating the AIE nature of probe in aqueous medium. The aggregate of **Mes-BOD-SePh** shows green fluorescence at 526 nm.

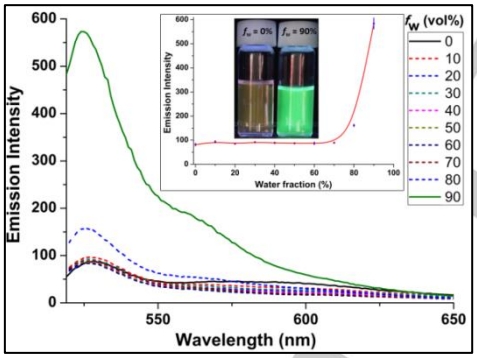


**Figure 8.** Fluorescence spectra of Mes-BOD-SePh in THF-water mixtures with different water fractions ($f_w$); Inset: Plots of emission intensity vs water fractions, and fluorescence images at $f_w$ = 0% and 90%.

## Conclusions

Herein, we have studied the substituent effect at the *meso* position on the BODIPY framework. The synthesized phenyl selenide-based BODIPY (**Mes-BOD-SePh**) probe shows fast and selective turn-on response to the hypochlorous acid over other ROS/RNS. The probes display excellent selectivity, sensitivity, as well as short time responses (~1-2 min.) for hypochlorite in physiological pH. **Mes-BOD-SePh** showed fluorescence enhancement of up to ~110 fold with detection limits at 19.6 nM. Incorporation of mesitylene group at the *meso* position of BODIPY framework not only helps to increase the fluorescence enhancement and photostability, but helps to selectively carry the probe into the lipid droplets. This study tells how a substituent effect on the fluorophore allows for different behavior of the probe under physiological conditions such as in cell imaging experiments.

## Experimental Section

General considerations: All chemicals used herein were used as received from commercial suppliers (Aldrich, Tokyo Chemical Industry). $^{1}$H, $^{13}$C, $^{77}$Se NMR spectra were acquired using a Bruker Avance 400 and Agilent-NMR-vnmrs 600 MHz spectrometer. TMS and dimethyl selenide was used as external standards. ESI-mass spectrometry was performed on a BRUKER micrOTOF-Q Ⅱ by the research support staff at KAIST. A Time-of-Flight mass spectrometer was operated at a resolution of 20,000 Absorption spectra and stopped-flow absorption spectra were measured using a JASCO V–530 and JASCO-815Uv/Vis spectrophotometer, respectively. Fluorescence measurements were carried out with a Shimadzu RF–5301pc spectrofluorophotometer.

**Synthesis of 2:**

To a solution of 2,4,6-trimethylbenzaldehyde (**1**) (148 mg, 1.0 mmol, 1 equiv) in dry $CH_2Cl_2$ (25 mL) were added 2,4–dimethylpyrrole (0.23 mL, 2.2 mmol, 2.2 equiv) and a catalytic amount of TFA (0.05 mL) at room temperature and stirred for 6 h under nitrogen. Then, DDQ (227 mg, 1.0 mmol) was added to the reaction mixture; the contents were then stirred at room temperature for 30 min. Triethylamine (0.42 mL, 3.0 mmol) was added to the reaction mixture and the mixture was stirred for a further 10 min. $BF_3OEt_2$ (0.37 mL, 3.0 mmol) was added to the reaction mixture and stirred for an additional 3 h at room temperature. Then, the reaction was quenched with water (25 mL) and aqueous layer extracted with $CH_2Cl_2$ (3 × 25 mL). The combined organic layers were washed with brine, dried ($Na_2SO_4$) and concentrated under vacuum. The crude product was purified by silica gel column chromatography using hexane and $CH_2Cl_2$ (3:1) to give **2** as an orange solid (230 mg, 62%); M.P. = 121-122 °C; IR ($CHCl_3$) ῡ = 2923, 2855, 2361, 2339, 2213, 1539, 1472, 1441, 1404, 1354, 1310, 1250, 1183, 1126, 1095, 1065, 1002, 911, 854, 821, 778, 733, 705 cm$^{-1}$; $^{1}$H-NMR (400 MHz, $CDCl_3$/TMS): δ = 1.38 (s, 6H, $H_{11,13}$), 2.09 (s, 6H, $H_{19}$), 2.33 (s, 3H, $H_{20}$), 2.56 (s, 6H, $H_{12,14}$), 5.96 (s, 2H, $H_{2,6}$), 6.95 (s, 2H, $H_{17}$); $^{13}$C-NMR (100 MHz, $CDCl_3$): δ = 13.5 ($C_{11,13}$), 14.7 ($C_{12,14}$), 19.6 ($C_{19}$), 21.3 ($C_{20}$), 120.9 ($C_{2,6}$), 129.1 ($C_{17}$), 130.7 ($C_{8,10}$), 131.2 ($C_{15}$), 135.0 ($C_{16}$), 138.7 ($C_{18}$), 141.8 ($C_9$), 142.4 ($C_{1,7}$), 155.2 ($C_{2,5}$); $^{11}$B-NMR (128.4 MHz, $CDCl_3$): δ = 0.68 (t, $J_{B-F}$ = 34.9 Hz); $^{19}$F-NMR (376.5 MHz, CDCl3): δ = –146.2 (q, $J_{F-B}$ = 33.0 Hz);HRMS (ESI): calcd for $C_{22}H_{25}BF_2N_2$ + Na: 389.1977, found: m / z 389.1980 (M + Na)$^+$.

**Synthesis of 3:**

To a stirred solution of **2** (183 mg, 0.5 mmol) in hexafluoro-2-propanol (HFIP, 4 mL) was added *N*-chlorosuccinimide (73 mg, 0.55 mmol, 1.1 equiv). The reaction mixture was stirred at room temperature for 15 min (reaction monitored by TLC). Then, the solvent was evaporated under reduced pressure; the residue was diluted with $CH_2Cl_2$ (30 mL). The organic layer was washed with water (2 × 10 mL), dried ($Na_2SO_4$) and concentrated under vacuum. The crude product was purified by silica gel column chromatography using hexane and $CH_2Cl_2$ (3:1) to afford **3** as an orange solid (160 mg, 80%). M.P. = 90-91 °C; IR ($CHCl_3$) ῡ = 2923, 2855, 2361, 2339, 2213, 1611, 1539, 1472, 1441, 1404, 1354, 1310, 1250,

1183, 1126, 1095, 1065, 1002, 911, 854, 821, 778, 733, 705 $cm^{-1}$; $^{1}$H-NMR (400 MHz, $CDCl_3$/TMS): δ = 1.37 (s, 3H, $H_{11}$), 1.39 (s, 3H, $H_{13}$), 2.08 (s, 6H, $H_{19}$), 2.34 (s, 3H, $H_{20}$), 2.57 (s, 6H, $H_{12,14}$), 6.01 (s, 1H, $H_6$), 6.96 (s, 2H, $H_{17}$); $^{13}$C-NMR (100 MHz, $CDCl_3$): δ = 10.7 ($C_{11}$), 12.3 ($C_{12}$), 13.7 ($C_{13}$), 14.9 ($C_{14}$), 19.6 ($C_{19}$), 21.3 ($C_{20}$), 121.2 ($C_2$), 121.8 ($C_6$), 128.3 ($C_{10}$), 129.2 ($C_{17}$), 130.8 ($C_{15}$), 131.5 ($C_8$), 135.0 ($C_{16}$), 135.6 ($C_1$), 139.0 ($C_{18}$), 142.2 ($C_9$), 144.3 ($C_7$), 149.8 ($C_3$), 157.7 ($C_5$); $^{11}$B-NMR (128.4 MHz, $CDCl_3$): δ = 0.51 (t, $J_{B-F}$ = 34.1 Hz); $^{19}$F-NMR (376.5 MHz, CDCl3): δ = –146.5 (q, $J_{F-B}$ = 32.5 Hz); HRMS (ESI): calcd for $C_{22}H_{24}BClF_2N_2$ + Na: 423.1587, found: m / z 423.1582 $(M + Na)^+$.

**Synthesis of Mes-BOD-SePh:**

To a stirred solution of **3** (100 mg, 0.25 mmol) in dry $CH_2Cl_2$ (10 mL) was added PhSeCl (48 mg, 0.25 mmol, 1.0 equiv). The reaction mixture was stirred at room temperature for 30 min (reaction monitored by TLC). Then, the solvent was evaporated under reduced pressure and the crude product was purified by silica gel column chromatography using hexane and $CH_2Cl_2$ (3:1) to afford **Mes-BOD-SePh** as a red solid (123 mg, 89%). M.P. = 161-162 °C; IR ($CHCl_3$) ῡ = 2957, 2922, 2859, 2735, 2361, 1669, 1653, 1612, 1543, 1507, 1472, 1437, 1411, 1364, 1306, 1251, 1194, 1156, 1129, 1121, 1084, 1048, 981, 850, 807, 778, 757, 704 $cm^{-1}$; $^{1}$H-NMR (400 MHz, $CDCl_3$/TMS): δ = 1.40 (s, 3H, $H_{11}$), 1.50 (s, 3H, $H_{13}$), 2.09 (s, 6H, $H_{19}$), 2.34 (s, 3H, $H_{20}$), 2.61 (s, 3H, $H_{12}$), 2.67 (s, 3H, $H_{14}$), 6.97 (s, 2H, $H_{17}$), 7.11-7.20 (m, 5H, $H_{21,22,23}$); $^{13}$C-NMR (100 MHz, $CDCl_3$): δ = 11.0 ($C_{11}$), 12.6 ($C_{12}$), 13.8 ($C_{13}$), 14.5 ($C_{14}$), 19.7 ($C_{19}$), 21.4 ($C_{20}$), 118.1 ($C_6$), 122.6 ($C_2$), 126.1 ($C_{24}$), 128.8 ($C_{23}$), 128.9 ($C_8$), 129.1 ($C_{10}$), 129.38 ($C_{22}$), 129.42 ($C_{17}$), 130.8 ($C_{15}$), 132.5 ($C_{21}$), 134.8 ($C_{16}$), 137.4 ($C_1$), 139.3 ($C_{18}$), 142.9 ($C_9$), 147.6 ($C_7$), 152.3 ($C_3$), 159.9 ($C_5$); $^{77}$Se-NMR (76.3 MHz, $CDCl_3$): δ =205.4; $^{11}$B-NMR (128.4 MHz, $CDCl_3$): δ = 0.52 (t, $J_{B-F}$ = 33.5 Hz); $^{19}$F-NMR (376.5 MHz, CDCl3): δ = –146.1 (q, $J_{F-B}$ = 32.0 Hz); HRMS (ESI): calcd for $C_{28}H_{28}BClF_2N_2Se$ + Na: 579.1065, found: m / z 579.1052 $(M + Na)^+$.

**Cell culture and fluorescence imaging.**

Human adipose stem cells (hADSC) were cultured in DMEM supplemented with 10 % fetal bovine serum (Gibco) and 1 % penicillin/streptomycin (100 U/mL, Gibco). The hADSC seeded at a density of $2\times10^5$ cells on sterilized 18 mm$\Phi$ cover-slips in a 12-well cell culture plate and was maintained at 37 °C in a 5 % $CO_2$ humidified incubator. Fluorescent images were acquired on a Zeiss LSM 780 laser scanning confocal microscope were used. The excitation wavelength was 488 nm; the detection wavelength was 490-553 nm. The DNA in the cell nucleus was stained with DRAQ5 (Thermo Scientific). Prior to imaging, the culture medium was removed and cells were washed with D-PBS three times.

**Cell viability assays.**

The proliferation of human adipose stem cells (hADSC) was determined by WST-1 assay kit (Roche) with the manufacturer's protocols. The human adipose stem cells pre-treated with the **Mes-BOD-SePh** at various concentrations (1, 2.5, 7.5, 10, 25, 50 μM) and control cells were seeded with $5 \times 10^3$ cells / well in 96-well plate (n = 6). The cells proliferation reagent WST-1 was added (10 μL) to each well and the reagent-applied cells were incubated for 2 h at 37°C, 5% $CO_2$. Absorbances were measured using a VersaMax ELISA microplate ELISA reader at 450 nm and the reference wavelength was 590 nm.

**DFT calculations.**

Optimized structures and HOMO–LUMO distributions of the states were estimated using DFT/TDDFT calculations using the Gaussian 09 program. The B3LYP functional with a 6–31g* basis set was used and the 6–311g* basis set was used for Se only. All calculations were performed in the gas phase. Configuration interaction (CI) coefficients were obtained by square of the values.

## Acknowledgements

The Molecular Logic Gate Laboratory operated by Prof. D. G. Churchill acknowledges support from the Mid-Career Researcher Program through the NRF (National Research Foundation) of Korea (NRF-2014R1A2A1A11052980) funded by MEST, HRHR program from KAIST, and the Institute for Basic Science (IBS) for financial support. Dr. S. V. Mulay and Y. Kim acknowledge IBS research fellowships and KAIST for providing research facilities. Tesla Yudhistira acknowledge Lembaga Pengelola Dana Pendidikan (LPDP) Indonesia Endownment Fund for the fellowship and KAIST for providing research facilities. The research support staff at KAIST facilitated the acquisition of MS data.

**Keywords:** BODIPY • Fluorescent probe • Hypochlorous acid • Lipid droplet • Aggregation induced emission

[1] a) T. Finkel, N. J. Holbrook, *Nature* **2000**, *408*, 239-247; b) A. Gomes, E. Fernandes, J. L. Lima, *J. Biochem. Biophys. Methods* **2005**, *65*, 45-80.
[2] X. Li, G. Zhang, H. Ma, D. Zhang, J. Li, D. Zhu, *J. Am. Chem. Soc.* **2004**, *126*, 11543-11548.
[3] a) Z. M. Prokopowicz, F. Arce, R. Biedron, C. L. Chiang, M. Ciszek, D. R. Katz, M. Nowakowska, S. Zapotoczny, J. Marcinkiewicz, B. M. Chain, *J. Immunol* **2010**, *184*, 824-835; b) Y.-C. Yang, H.-H. Lu, W.-T. Wang, I. Liau, *Anal. Chem.* **2011**, *83*, 8267-8272.
[4] M. B. Hampton, A. J. Kettle, C. C. Winterbourn, *Blood* **1998**, *92*, 3007-3017.
[5] J. M. Pullar, M. C. M. Vissers, C. C. Winterbourn, *IUBMB Life*, **2000**, *50*, 259-266.
[6] a) D. I. Pattison, M. J. Davies, *Chem. Res. Toxicol.* **2001**, *14*, 1453-1464; b) S. M. Wu, S. V. Pizzo, *Arch. Biochem. Biophys.* **2001**, *391*, 119-126; c) M. J. Steinbeck, L. J. Nesti, P. F. Sharkey, J. Parvizi, *J Orthop. Res.* **2007**, *25*, 1128-1135.
[7] T. Hasegawa, E. Malle, A. Farhood, H. Jaeschke, *Am. J. Physiol. Gastrointest. Liver Physiol.* **2005**, G760–G767,.
[8] A. Daugherty, J. L. Dunn, D. L. Rateri, J. W. Heinecke, *J. Clin. Invest.* **1994**, *94*, 437-444.
[9] Y. W. Yap, M. Whiteman, N. S. Cheung, *Cell. Signal.* **2007**, *19*, 219-228.
[10] S. Hammerschmidt, N. Buchler, H. Wahn, *Chest* **2002**, *2*, 573-581.
[11] S. Sugiyama, K. Kugiyama, M. Aikawa, S. Nakamura, H. Ogawa, P. Libby, *Arterioscler. Thromb. Vasc. Biol.* **2004**, *24*, 1309-1314.
[12] a) D. L. Brasaemle, *J. Lipid Res.* **2007**, *48*, 2547-2559; b) P. E. Bickel, J. T. Tansey, M. A. Welte, *Biochim. Biophys. Acta* **2009**, *1791*, 419-440; c) T. C. Walther, R. V. Farese, Jr., *Annu. Rev. Biochem.* **2012**, *81*, 687-714.
[13] P. T. Bozza, I. Bakker-Abreu, R. A. Navarro-Xavier, C. Bandeira-Melo, *Prostaglandins Leukot. Essent. Fatty Acids* **2011**, *85*, 205-213.
[14] A. K. Stobart, S. Stymne, S. Hoglund, *Planta* **1986**, *169*, 33-37.
[15] a) C.-L. E. Yen, S. J. Stone, S. Koliwad, C. Harris, R. V. Farese, Jr., *J. Lipid Res.* **2008**, *49*, 2283-2301; b) A. S. Greenberg, R. A. Coleman, F. B. Kraemer, J. L. McManaman, M. S. Obin, V. Puri, Q. W. Yan, H.

Miyoshi, D. G. Mashek, *J. Clin. Invest.* **2011**, *121*, 2102-2110; c) R. Zechner, R. Zimmermann, T. O. Eichmann, S. D. Kohlwein, G. Haemmerle, A. Lass, F. Madeo, *Cell Metab.* **2012**, *15*, 279-291.

[16] R. Bartz, J. K. Zehmer, M. Zhu, Y. Chen, G. Serrero, Y. Zhao, P. Liu, *J. Proteome Res.* **2007**, *6*, 3256-3265.

[17] M. A. Welte, *Trends Cell. Biol.* **2007**, *17*, 363-369.

[18] L. Yang, Y. Ding, Y. Chen, S. Zhang, C. Huo, Y. Wang, J. Yu, P. Zhang, H. Na, H. Zhang, Y. Ma, P. Liu, *J. Lipid Res.* **2012**, *53*, 1245-1253.

[19] A. Herms, M. Bosch, N. Ariotti, B. J. N. Reddy, A. Fajardo, A. Fernandez-Vidal, A. Alvarez-Guaita, M. A. Fernandez-Rojo, C. Rentero, F. Tebar, C. Enrich, M.-I. Geli, R. G. Parton, S. P. Gross, A. Pol, *Curr. Biol.* **2013**, *23*, 1489-1496.

[20] I. Hapala, E. Marza, T. Ferreira, *Biol. Cell* **2011**, *103*, 271-285.

[21] A. Vallet-Pichard, V. Mallet, S. Pol, *Semin Liver Dis.* **2012**, *32*, 158-166.

[22] M. Akiyama, D. Sawamura, Y. Nomura, M. Sugawara, H. Shimizu, *J. Invest. Dermatol.* **2003**, *121*, 1029-1034.

[23] F. B. Gonzaga, L. R. Cordeiro, *Accred. Qual. Assur.* **2014**, *19*, 283-287.

[24] A. F. Krivis, E. S. Gazda, *Anal. Chem.* **1967**, *39*, 226–227.

[25] M. Murata, T. A. Ivandini, M. Shibata, S. Nomura, A. Fujishima, Y. Einaga, *J. Electroanal. Chem.* **2008**, *612*, 29-36.

[26] a) A. P. de Silva, T. S. Moody, G. D. Wright, *Analyst* **2009**, *134*, 2385–2393; b) Z. Xu, J. Yoon, D. R. Spring, *Chem. Soc. Rev.* **2010**, *39*, 1996-2006; c) J. Du, M. Hu, J. Fan,, X. Peng, *Chem. Soc. Rev.* **2012**, *41*, 4511-4535; d) G. Chen, F. Song, X. Xiong, X. Peng, *Ind. Eng. Chem. Res.* **2013**, *52*, 11228-11245; e) J. Fan, M. Hu, P. Zhan, X. Peng, *Chem. Soc. Rev.* **2013**, *42*, 29-43; f) Y. Zhou, J. F. Zhang, J. Yoon, *Chem. Rev.* **2014**, *114*, 5511-5571; g) Z. Lou, P. Li, K. Han, *Acc. Chem. Res.* **2015**, *48*, 1358-1368; h) H. Zhu, J. Fan, B. Wang, X. Peng, *Chem. Soc. Rev.* **2015**, *44*, 4337-4366.

[27] a) A. Loudet, K. Burgess, *Chem.. Rev.* **2007**, 4891−4932; b) G. Ulrich, R. Ziessel, A. Harriman, *Angew. Chem. Int. Ed.* **2008**, *47*, 1184-1201; c) A. Bessette, G. S. Hanan, *Chem. Soc. Rev.* **2014**, *43*, 3342-3405; d) J.-T. Hou, M.-Y. Wu, K. Li, J. Yang, K.-K. Yu, Y.-M. Xie, X.-Q. Yu, *Chem. Commun.* **2014**, *50*, 8640-8643; e) T. Kowada, H. Maeda, K. Kikuchi, *Chem. Soc. Rev.* **2015**, *44*, 4953-4972.

[28] a) S. Kenmoku, Y. Urano, H. Kojima, T. Nagano, *J. Am. Chem. Soc.* **2007**, *129*, 7313-7318; b) X. Chen, K.-A. Lee, E.-M. Ha, K. M. Lee, Y. Y. Seo, H. K. Choi, H. N. Kim, M. J. Kim, C.-S. Cho, S. Y. Lee, W.-J. Lee, J. Yoon, *Chem. Commun.* **2011**, *47*, 4373-4375; c) Y. Koide, Y. Urano, K. Hanaoka, T. Terai, T. Nagano, *J. Am. Chem. Soc.* **2011**, *133*, 5680-5682; d) L. Yuan, W. Lin, Y. Xie, B. Chen, J. Song, *Chem. Eur. J.* **2012**, *18*, 2700-2706; e) X. Wu, Z. Li, L. Yang, J. Han, S. Han, *Chem. Sci.* **2013**, *4*, 460-467; f) Q. Xu, K.-A. Lee, S. Lee, K. M. Lee, W.-J. Lee, J. Yoon, *J. Am. Chem. Soc.* **2013**, *135*, 9944-9949; g) R. Zhang, Z. Ye, B. Song, Z. Dai, X. An, J. Yuan, *Inorg. Chem.* **2013**, *52*, 10325-10331; h) H. Xiao, K. Xin, H. Dou, G. Yin, Y. Quan, R. Wang, *Chem. Commun.* **2015**, *51*, 1442-1445.

[29] X. Chen, X. Wang, S. Wang, W. Shi, K. Wang, H. Ma, *Chem. Eur. J.* **2008**, *14*, 4719-4724.

[30] a) Z.-N. Sun, F.-Q. Liu, Y. Chen, P. K. H. Tam, D. Yang, *Org. Lett.* **2008**, *10*, 2171-2174; b) J. J. Hu, N.-K. Wong, Q. Gu, X. Bai, S. Ye, D. Yang, *Org. Lett.* **2014**, *16*, 3544-3547.

[31] a) W. Lin, L. Long, B. Chen, W. Tan, *Chem. Eur. J.* **2009**, *15*, 2305-2309; b) X. Cheng, H. Jia, T. Long, J. Feng, J. Qin, Z. Li, *Chem. Commun.* **2011**, *47*, 11978-11980; c) N. Zhao, Y.-H. Wu, R.-M. Wang, L.-X. Shi, Z.-N. Chen, *Analyst* **2011**, *136*, 2277-2282; d) M. Emrullahoglu, M. Ucuncu, E. Karakus, *Chem. Commun.* **2013**, *49*, 7836-7838.

[32] a) T.-I. Kim, S. Park, Y. Choi, Y. Kim, *Chem. Asian J.* **2011**, *6*, 1358-1361; b) G. Li, D. Zhu, Q. Liu, L. Xue, H. Jiang, *Org. Lett.* **2013**, *15*, 2002-2005; c) S.-R. Liu, S.-P. Wu, *Org. Lett.* **2013**, *15*, 878-881; d) K. Xu, M. Qiang, W. Gao, R. Su, N. Li, Y. Gao, Y. Xie, F. Kong, B. Tang, *Chem. Sci.* **2013**, *4*, 1079; e) G. Cheng, J. Fan, W. Sun, J. Cao, C. Hu, X. Peng, *Chem. Commun.* **2014**, *50*, 1018-1020; f) S. T. Manjare, Y. Kim, D. G. Churchill, *Acc. Chem. Res.* **2014**, *47*, 2985-2998; g) Z. Lou, P. Li, K. Han, *Acc. Chem. Res.* **2015**, *48*, 1358-1368; h) S. Panda, A. Panda, S. S. Zade, *Coord. Chem. Rev.* **2015**, *300*, 86-100; i) Z. Qu, J. Ding, M. Zhao, P. Li, *J. Photochem. Photobiol. A* **2015**, *299*, 1-8; j) W. Zhang, W. Liu, P. Li, J. kang, J. Wang, H. Wang B. Tang, *Chem. Commun.* **2015**, *51*, 10150-10153; k) S. V. Mulay, M. Choi, Y. J. Jang, Y. Kim, S. Jon, D. G. Churchill, *Chem. Eur. J.* **2016**, *22*, 9642-9648; l) P. Venkatesan, S.-P. Wu, *Analyst* **2015**, *140*, 1349-1355.

[33] a) S. Goswami, S. Paul, A. Manna, *Dalton Trans.* **2013**, *42*, 10097-10101; b) S. Goswami, A. Manna, S. Paul, C. K. Quah, H.-K. Fun, *Chem. Commun*, **2013**, *49*, 11656-11658; c) S. Goswami, A. K. Das, A. Manna, A. K. Maity, P. Saha, C. K. Quah, H.-K. Fun, H. A. Abdel-Aziz, *Anal. Chem.* **2014**, *86*, 6315-6322; d) Z. Ye, R. Zhang, B. Song, Z. Dai, D. Jin, E. M. Goldys, J. Yuan, *Dalton Trans.* **2014**, *43*, 8414-8420; e) Y.-R. Zhang, X.-P. Chen, J. Shao, J.-Y. Zhang, Q. Yuan, J.-Y. Miao, B.-X. Zhao, *Chem. Commun.* **2014**, *50*, 14241-14244; f) H. Zhu, J. Fan, J. Wang, H. Mu, X. Peng, *J. Am. Chem. Soc.* **2014**, *136*, 12820-12823; g) J.-T. Hou, K. Li, J. Yang, K.-K. Yu, Y.-X. Liao, Y.-Z. Ran, Y.-H. Liu, X.-D. Zhou, X.-Q. Yu, *Chem. Commun.* **2015**, *51*, 6781-6784; h) Q. Xu, C. H. Heo, G. Kim, H. W. Lee, H. M. Kim, J. Yoon, *Angew. Chem. Int. Ed.* **2015**, *54*, 4890-4894; i) L. Yuan, L. Wang, B. K. Agrawalla, S.-J. Park, H. Zhu, B. Sivaraman, J. Peng, Q.-H. Xu, Y.-T. Chang, *J. Am. Chem. Soc.* **2015**, *137*, 5930-5938; j) J. Zhou, L. Li, W. Shi, X. Gao, X. Li, H. Ma, *Chem. Sci.* **2015**, *6*, 4884-4888.

[34] a) K. Kim, C. Jo, S. Easwaramoorthi, J. Sung, D. H. Kim, D.G. Churchill, *Inorg. Chem*, **2010**, *49*, 4881-4894; b) S. T. Manjare, J. Kim, Y. Lee, D. G. Churchill, *Org. Lett.* **2014**, *16*, 520-523; c) S. T. Manjare, S. Kim, W. D. Heo, D. G. Churchill, *Org. Lett.* **2014**, *16*, 410-412; d) D. P. Murale, S. T. Manjare, Y. S. Lee, D. G. Churchill, *Chem. Commun.* **2014**, *50*, 359-361; e) Y. Kim, S. V. Mulay, M. Choi S. B. Yu, S. Jon, D. G. Churchill, *Chem. Sci.* **2015**, *6*, 5435-5439; f) Y Kim, M. Choi, S. T. Manjare, S. Jon, D. G. Churchill, *RSC. Adv.* **2016** *6*, 32013-32017.

[35] R. P. Sabatini, B. Lindley, T. M. McCormick, T. Lazarides, W. W. Brennessel, D. W. McCamant, R. Eisenberg, *J. Phys. Chem. B* **2016**, *120*, 527-534.

[36] D. M. Wong, A. K. Franz, *J. Microbiol. Methods* **2013**, *95*, 122-128.

[37] Z. Wang, C. Gui, E. Zhao, J. Wang, X. Li, A. Qin, Z. Zhao, Z. Yu, B. Z. Tang, *ACS Appl. Mater. Interfaces* **2016**, *8*, 10193−10200.

10.1002/asia.201601400


WILEY-VCH

# FULL PAPER

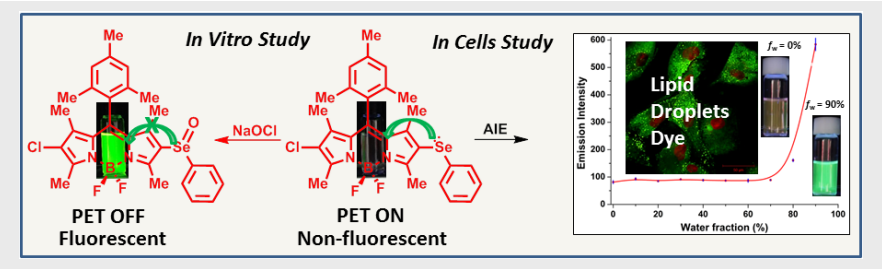


*Sandip V. Mulay, Tesla Yudhistira, Minsuk Choi, Youngsam Kim, Jinjoo Kim, Yoon Jeong Jang, Sangyong Jon and David G. Churchills**

***Page No. – Page No.***

**Substituent Effects in BOBIPY in Live Cell Imaging**

In this work, we presented how substituents on the BODIPY play significant roles for the detection of biologically important analytes under in vitro conditions and in live cell imaging studies. The probe shows selective and sensitive *turn-on* response with NaOCl over other ROS/RNS under in vitro conditions. Surprisingly, in live cell experiments, the probe specifically accumulates in lipid droplets and shows fluorescence turn-on responses because of aggregation-induced emission (AIE) due to the lipophilic mesitylene group at the *meso* position of the BODIPY.